Volume 1 | Number 1 | Jan 2013 | Pages 1–100

PCCP

Physical Chemistry Chemical Physics
www.rsc.org/pccp

ROYAL SOCIETY OF CHEMISTRY

ROYAL SOCIETY OF CHEMISTRY

www.rsc.org/pccp

Ab initio **theoretical investigation of beryllium and beryllium hydride nanoparticles and nanocrystals with implications for the corresponding infinite systems**

Aristides D. Zdetsis[*1,2], Michael M. Sigalas[3], Emmanuel N. Koukaras[1,4]

[1]Molecular Engineering Laboratory, Department of Physics, University of Patras, Patras 26500 GR, Greece

[2] Institute of Electronic Structure and Laser, Foundation for Research &Technology Hellas, Vassilika Vouton, P.O. Box 1385, Heraklion, Crete GR-71110, Greece

[3]Department of Materials Science, University of Patras, Patras 26500 GR, Greece

[4] Institute of Chemical Engineering Sciences, Foundation for Research and Technology Hellas, (FORTH/ICE-HT), Patras GR-26504, Greece

ABSTRACT

With the initial motivation of optimizing hydrogen storage in beryllium nanocrystals, we have thoroughly and systematically studied the structural and cohesive and electronic properties of Be_n and Be_nH_{xn} (n=2-160, x=0.1-2.4) nanoparticles as a function of both size (*n*) and hydrogen content (*x*), using density functional theory with a properly selected meta-hybrid functional and high level coupled clusters CCSD(T) theory for comparison. We have calculated the binding energies of Be_n, Be_nH_{xn} and $[BeH_2]_n$ nanoparticles for a large range of n values. In the limit n→∞, we have obtained the experimental binding energy of Be crystal (3.32 eV) with unexpectedly very good agreement (3.26±0.06 eV), and a predicted value of 7.85 eV ±0.02 eV

for the binding energy of for $[BeH_2]_\infty$ infinite system. We also predict that the majority of the lowest energy stoichiometric Be_nH_{2n} nanoparticles are chains or chain-like structures. The tendency towards chain stabilization of Be_nH_{xn} nanoparticles increases, as x approaches the stoichiometric value x=2, leading for large values of n, as n$\rightarrow\infty$, to polymeric forms of bulk BeH_2, which in the past have been considered as the leading forms of solid BeH_2. For such 1-dimensional forms of $[BeH_2]_n$ we have obtained and verified that the binding energy varies exactly proportionally to n^{-1}. The extrapolated desorption energy for such polymeric forms of solid BeH_2 is found to be 19±3 kJ/mol in juxtaposition to the experimental value of 19 kJ/mol for solid BeH_2, suggesting that the difference ΔE in cohesive energy between the orthorhombic and polymeric form is very small ($\Delta E \approx$ 3 kJ/mol). This is in full accord with the early discrepancies in the literature in determining and distinguishing the real crystal structure of solid BeH_2.

*corresponding author: zdetsis@upatras.gr

TOC Graphic
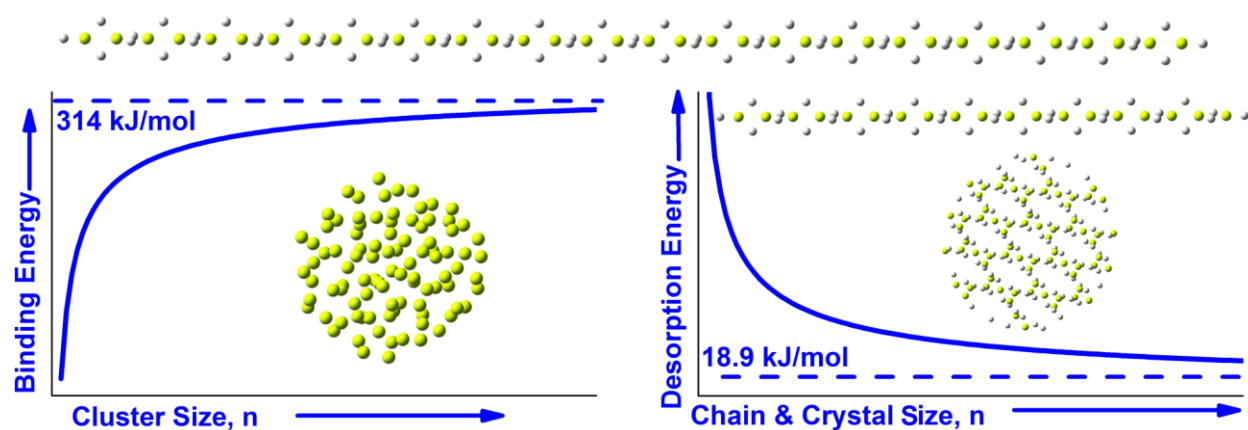
Using judicially chosen DFT calculations for Be_n and Be_nH_x nanoparticles we predict correctly the n$\rightarrow\infty$ behavior for crystals and polymers.

1. Introduction

It has been suggested recently that metal and metal-hydride nanoparticles could be more efficient for hydrogen storage (which is a very important and hot problem in materials research), compared to their corresponding bulk materials [1-9]. This has stimulated a lot of interest in the investigation of metal hydride nanoparticles [6-9] and in particular into their hydrogen storage capabilities, which involves the study of the corresponding metal nanoparicles as well. Although this was our initial motivation, in the process of our investigation and in view of our recent results for MgH_2 in which from the study of the nanocrystals we were lead to extremely good predictions for the infinite MgH_2 solid [9], the focus of our current work has been shifted towards predictions for the infinite systems based on the rationalized study of the corresponding nanoparticles. Obviously, hydrogen storage is a remote target in both cases. Hydrogen is an ideal fuel since it has about three times higher gravimetric energy density than petrol [1,2]. Taking into account the limiting availability of hydrocarbons (as opposed to abundance of hydrogen) and the significant environmental effect of burning hydrocarbons (in contrast, there is minimal pollution from hydrogen fuel), it is clear that there is significant interest and research in this area. [1] However, a major obstacle towards widespread application of hydrogen fuels is their storage. [1–5] Certain targets have been set for the volumetric and gravimetric hydrogen densities of the storage materials. [1] One extensively studied category of possible materials, which are close at meeting those targets, is metal hydrides [2–9], among which magnesium hydride as well as beryllium hydride have a particular importance (each, for different reasons). For example, a group of Mg-based hydrides can have reversible hydrogen capacity of up to 7.6 wt% meeting the targets, although they exhibit slow kinetics and high desorption temperatures making them impractical [2]. BeH_2 on the other hand, has a high hydrogen storage capacity (18.2 wt %), but it

has been ruled out as a solid hydride for commercial hydrogen storage material because of its high toxicity. Yet, it has still attracted considerable interest as rocket fuel and for nuclear reactors [10].

A possible way to improve MgH_2 problems, which are common to many metal hydrides (including BeH_2), is using nanostructured metal hydrides [5–9]. Due to the significantly increased surface to volume ratio, reaction kinetics is expected to improve and possibly desorption energies to be reduced [7–9]. This is in part true, as we have shown in our previous study for Mg_nH_m nanoclusters and nanocrystals [9], in which all such possibilities have been tested. Yet, each system has its own peculiarities, due to the central role of the relative strength of the hydrogen-metal over the metal-metal interaction. In view of its very lightweight, beryllium is a next very promising candidate for examining the possible consequences of "miniaturization" in desorption energies. Thus, in the present work, expanding our previous theoretical study of Mg nanostructured hydrides, [9] we have performed an analogous high quality study of Be nanostructured hydrides.

Bare beryllium clusters Be_n (and in particular small clusters with n up to 21 atoms) have been extensively studied computationally in the literature [11-12], because, in addition to their fundamental chemical interest and light weight, they also constitute excellent testing systems for comparing the capabilities of different computational methods and schemes. The earliest calculations of interaction between hydrogen atoms and beryllium clusters [13] used the simple Hartree-Fock (check) self-consistent field (SCF) method with contracted Gaussian basis-functions. They found that the chemisorbed bond energies of hydrogen in at least three of the sites studied were about 40 kcal/mol. However, as expected in such an early study, the accuracy could be rather limited, especially in the determination of the lowest-energy-structures and

4

energies of the bare Be clusters. The Be_nH_{2n} clusters are known [10, 14] to form a long chain

structure (oligomers), the structural properties and electronic properties of which and band gap

values have been studied using density functional theory (DFT) within the generalized gradient

approximation (GGA) employing the hybrid B3LYP functional [10], and the pseudopotential

plane-wave approach [14]. In a recent work [15] $Mg_mC_nH_x$ and $Be_mC_nH_x$ clusters were

generated by laser ablation, and studied both experimentally and theoretically using both second

order Møller–Plesset perturbation theory (MP2), and DFT .

Significant studies have been also performed for the interaction of crystalline bulk Be with

hydrogen. The crystal structure of beryllium hydride, BeH_2, has been determined using high-

resolution powder diffraction data, and was found to correspond to space groups Ibam or Iba2

[16]. Ab initio calculations of hydrogen in different lattice positions in bulk Be as well as in

vacancies of Be crystal have been reported [17], locating the most favorable energetically

positions of hydrogen, as well as the most probable diffusion pathways. There are also reports on

ab initio study of amorphous beryllium hydride for various concentrations of hydrogen [18].

Our present study of Be_nH_{nx} nanoparticles is part of a general ongoing direction on metal

hydrides, and a natural extension of our previous study on Magnesium hydride [9]. Similarly to

that study (ref 9), we are using modern density functional theory employing judicially chosen

high accuracy functionals and meta-functionals to study the analogous Be_n and Be_nH_m clusters in

order to find the corresponding binding and hydrogen desorption energies. Again, similarly to

the case of MgH_2, on the basis of comparisons with high level *ab initio* Coupled Clusters

calculations, including single, double (CCSD), and perturbative triple CCSD(T) excitations for

representative Be_n and Be_nH_m clusters, we have finally selected the M06 meta-functional, as will

be described in detail bellow. Using this meta-functional, we have calculated the total and binding energies of Be_n and Be_nH_{xn} (n=2-166, x=1-2.2) nanoclusters and nanocrystals very accurately. For instance, by suitably extrapolating the binding energy results of Be_n nanocrystals all the way to n→∞, we have obtained the experimental binding energy of 3.32 eV per atom for crystalline Be [18] with unexpectedly high accuracy (3.26±0.06 eV) per atom. This type of accuracy becomes even more intriguing in view of earlier theoretical results [18] obtained by sophisticated band structure methods, which obtained binding energy values from 3.60 eV per atom to 3.70 eV per atom. Furthermore, from our Be_nH_{2n} binding and H-desorption energies we have found that in most cases the nanochains are more stable than the corresponding nanoclusters and even larger nanocrystals. This is clearly related to the fact that polymeric and amorphous phases of solid BeH_2 are quite stable [10, 14] and relatively easy to prepare [18]. In fact, due to this high stability of chains, it was originally believed that the solid phase of BeH_2 was consisted of interconnected flat polymeric chains of bridging hydrides [18]. The established crystal structure of pure BeH_2 is body-centered orthorhombic with a network of connected (corner sharing) BeH_4 tetrahedra. There is no known analogue of such type of structure among other compounds containing tetrahedral building blocks, which complicates very much the construction of "pure crystalline nanocrystals". This is not totally unrelated, as will be further explained below, to a resulting "chain desorption energy" of 29 kJ/mol, compared to the bulk desorption energy of 19 kJ/mol. It is clear from this discussion, as will be would be shown below that the behavior of Be_nH_{xn} and Be_nH_{2n} nanoclusters and nanocrystals is dramatically different compared to the behavior of the corresponding Mg_nH_{xn} and Mg_nH_{2n} nanoparticles. The structure of the present paper is as follows: In the next section, section 2, we briefly present the theoretical and computational methods employed here. The results for pure Be_n nanoclusters are

6

discussed in section 3. In section 4 we present the results and discussion of small and medium Be_nH_m (m=xn) non-stoichiometric and stoichiometric clusters, and in section 5 we discuss the large stoichiometric Be_nH_{2n} nanocrystals and nanochains. Finally, in section 6 we summarize the conclusions of the present work for the whole variety of Be_nH_m and $[BeH_2]_n$ (n=2, … $\rightarrow$ ∞) nanocrystals and nanochains.

2. Theoretical approach and computational techniques

We have examined a large variety of free Be_n and Be_nH_m nanoclusters (n=2-19, m=2-n+2) and nanocrystals (n=36-166, m=2n) using all electron density functional theory with properly selected functionals. As in the case of Mg_nH_m clusters [9], the initial (before optimization) geometries of the lowest and lower energy bare Be_n clusters have been obtained from the literature [11, 19-20] and were optimized under no symmetry constrains. In contrast to nano-clusters, for the large size nanocrystals (n>30), for which a uniform bulk-like geometry is required (for the subsequent extrapolation to the infinite crystal) the initial geometries were obtained as spherical fragments of the bulk crystal. This seems to be the simplest, uniform, and most cost-effective method. For representative small clusters used as benchmarks such as Be_4, Be_4H_8, Be_7, Be_7H_{14}, these geometries were further optimized and reevaluated using a variety of functionals and meta-functionals together with *ab initio* many body Møller-Plesset perturbation theory of second order (MP2), and coupled-cluster theory, including single and double excitations (CCSD). In these cases at the equilibrium geometries single point energy calculations were performed using higher level methods, such as CCSD(T), which includes triple excitations non-iteratively. We should emphasize that beryllium clusters are challenging systems. The beryllium dimer is a well known example of multi-reference system, the proper treatment of

7

which eludes even highly accurate methods such as CCSD(T) [19]. Although the specific

problematic behavior is not directly transferred to larger systems, nevertheless the performance

of various functionals and meta-functionals varies substantially [20]. The functional of Perdew,

Burke and Ernzerhof, PBE [21] performs surprising well in reproducing the equilibrium

geometry of the beryllium dimer with a difference of 0.03 Å [22] compared to the experimental

value. [23] However, even though the calculated equilibrium lengths by the PBE functional are

exceptionally good, the corresponding binding energy is significantly overestimated [20, 22].

This is verified from our benchmark calculations described below. Therefore, for the majority of

nanoparticles the geometry optimizations were performed employing the PBE functional using

the def-TZVP [24] basis set which is of triple-ζ quality. At the equilibrium geometries, based on

our comparisons with the high level CCSD and CCSD(T) *ab initio* methods, we have performed

single point energy calculations using the highly parameterized meta-hybrid M06 [25] functional

with the larger correlation consistent (cc) cc-pVTZ basis set [26]. To arrive at this choice,

similarly to MgH_2, we have considered and compared with several other popular and modern

functionals and meta-functionals. Comparisons have been made for the Be_4, Be_4H_8, Be_7, Be_7H_{14}

test nanoparticles using generalized-gradient approximation (GGA), hybrid GGA, and hybrid

meta-GGA functionals, namely: B97-D, [27] B3LYP, [28,29] TPSSh, [30,31] M05, [32] M05-

2X, [32] and M06-2X [25], all incorporated in the GAUSSIAN program package [33] which was

used for the entire set of DFT and CCSD(T) calculations in the present study. Obviously, we

cannot use an exhaustive list of functionals, neither we can embark on an in-depth comparison of

various functionals, which would be completely out of the scope of the present investigation.

The main quantity of interest for the comparisons between functional is the desorption energy,

which is based on energy differences between hydrogenated and non-hydrogentated systems.

8

The absolute (not normalized) desorption or dissociation energy, $\Delta E_{dtot}(\mathrm{Be}_n\mathrm{H}_{2n})$, for a $\mathrm{Be}_n\mathrm{H}_{2n}$ nanocluster is defined as usual by the relation:

$$\Delta E_{dtot}(\mathrm{Be}_n\mathrm{H}_{2n}) = nE(\mathrm{H}_2) + [E(\mathrm{Be}_n) - E(\mathrm{Be}_n\mathrm{H}_{2n})] \tag{1}$$

Whereas the normalized per H_2 molecule desorption energy, $\Delta E_d(\mathrm{Be}_n\mathrm{H}_{2n})$, is given as:

$$\Delta E_d(\mathrm{Be}_n\mathrm{H}_{2n}) = E(\mathrm{H}_2) + [E(\mathrm{Be}_n) - E(\mathrm{Be}_n\mathrm{H}_{2n})]/n \tag{2}$$

In the above relations $E(\mathrm{H}_2)$, $E(\mathrm{Be}_n)$, and $E(\mathrm{Be}_n\mathrm{H}_{2n})$ are the total energies of the H_2 molecule, and of the Be_n and $\mathrm{Be}_n\mathrm{H}_{2n}$ clusters, respectively, including the zero-point energy (ZPE) corrections for all relevant structures (H_2, Be_n, and $\mathrm{Be}_n\mathrm{H}_{2n}$). As was explained elsewhere [9], the perfect outcome would lead to a functional which performs with systematic (not necessarily perfect) accuracy for both Be_n and $\mathrm{Be}_n\mathrm{H}_{2n}$ cases, and for small and large sizes. To this end, we compare the binding energies $E_b(\mathrm{Be}_n)$, and $E_b(\mathrm{Be}_n\mathrm{H}_{2n})$, of Be_n, and $\mathrm{Be}_n\mathrm{H}_{2n}$ clusters respectively :

$$E_b(\mathrm{Be}_n) = nE(\mathrm{Be}) - E(\mathrm{Be}_n) \quad (a), \quad E_b(\mathrm{Be}_n\mathrm{H}_{2n}) = nE(\mathrm{Be}) + 2nE(\mathrm{H}) - E(\mathrm{Be}_n\mathrm{H}_{2n}) \quad (b) \tag{3},$$

where $E(\mathrm{Be})$ and $E(\mathrm{H})$ are the atomic energies of Be and H respectively. The results of such comparisons for n=4 and 7, are summarized in Table 1.

For the non-stoichiometric $\mathrm{Be}_n\mathrm{H}_m$ clusters, the above definitions (1) and (2) are modified in an obvious way [9]:

$$\Delta E_d(\mathrm{Be}_n\mathrm{H}_m) = E(\mathrm{H}_2) + 2\left[E(\mathrm{Be}_n) - E(\mathrm{Be}_n\mathrm{H}_m)\right]/m \tag{4}$$

For such clusters, besides the "absolute" desorption energy defined above, we can consider the "stepwise desorption energy" ΔE_{sd} for the stepwise process:

9

$Be_nH_m \rightarrow Be_nH_{m-2} + H_2 \rightarrow Be_nH_{m-4} + 2H_2 \rightarrow ... \rightarrow Be_n + (m/2)H_2,$

in which a hydrogen molecule is removed (or added in the reverse process) at a time. In this case [9], we define the stepwise desorption energy ΔE_{sd} in relation to the energy of the Be_nH_{m-2} structure of the previous step, rather than with respect to the bare Be cluster:

$$\Delta E_{sd}(Be_nH_m) = E(H_2) + [E(Be_nH_{m-2}) - E(Be_nH_m)] \tag{5}$$

This definition can be further elaborated to "average stepwise desorption" of 2 and k steps [ref. 9].

For the results tabulated in Table 1, the geometry optimizations were performed by the coupled cluster CCSD method, and separately for each of the functionals in this Table, using the cc-pVTZ basis set [26]. Table 1 includes the binding energy, E_b, of the optimized structure as calculated using the corresponding functional, as well as the binding energy of each structure by a single point CCSD(T) calculation at the DFT optimized geometry. Our CCSD(T) results in Table 1 are in very good agreement to those provided by Sulka et al. [34], who have performed a detailed and exhaustive set of calculations for the binding energies of the small Be_n (n=2-6) clusters. For example, for Be_4 cluster the CCSD(T) binding energy we obtained here is 0.88 eV/atom, in comparison to the value of 0.8933 eV/atom obtained by Sulka et al. [34], at the complete basis set limit, with no frozen core, and no tight functions. It is also interesting to compare our calculated value of 1.076 eV/atom for the binding energy of the Be_7 cluster, with the values for Be_5 (1.0254 eV/atom) and Be_6 (1.0565 eV/atom) of Sulka et al. It is clear that a linear extrapolation of these results leads to a very good agreement with our Be_7 value (1.076/eV/atom).

TABLE 1. Binding energies (E_b) in eV of Be_4, Be_4H_8 and Be_7, Be_7H_{14} clusters, calculated with a variety of representative functionals, and CCSD(T) single point calculations at the corresponding DFT, and CCSD (last column) optimized geometries.

Structure	Property	PBE	B97D	TPSSh	B3LYP	M05-2X	M05	M06-2X	M06	CCSD
Be_4	De/cc-pVTZ (eV)	5.33	4.24	4.78	4.17	4.07	4.33	4.18	4.47	
	De/CCSD(T) (eV)	3.51	3.52	3.51	3.50	3.51	3.52	3.50	3.51	3.52
Be_4H_8	De/cc-pVTZ (eV)	31.18	31.23	32.67	31.78	30.74	30.35	31.21	31.69	
	De/CCSD(T) (eV)	30.11	30.11	30.11	30.11	30.11	30.10	30.10	30.10	30.11
Be_7	De/cc-pVTZ (eV)	11.20	8.96	10.20	8.86	8.99	9.82	9.29	9.73	
	De/CCSD(T) (eV)	7.55	7.79	7.54	7.52	7.53	8.05	7.51	7.52	7.53
Be_7H_{14}	De/cc-pVTZ (eV)	56.19	56.05	58.76	57.06	55.37	54.43	56.22	56.88	
	De/CCSD(T) (eV)	54.23	54.23	54.23	54.22	54.23	54.22	54.22	54.21	54.22

The energy values are indicative of the quality of both energy and the geometry. The quality of the geometries are good in all cases, with the best performance noted by the PBE functional and the worst (although not markedly), surprisingly, in the case of B3LYP. However, the PBE functional does not perform equally well with respect to energy values, being second worst only to the hybrid functionals TPSSh and B3LYP. As we can see, all selected functionals overestimate the binding energy in all cases. However, the Minnesota families of functionals M0x give binding energies nearest to the corresponding CCSD(T) values, followed by the B97-D functional of Grimme [27]. If computational efficiency and economy is taken into account the B97-D functional becomes a very attractive choice for these systems. The most systematic behavior between hydrogenated and non-hydrogenated clusters, also taking into account size

dependency, is observed for the M06 functional followed by M06-2X. In both cases the difference from the CCSD(T) binding energy values decreases going from the $n=4$ to $n=7$ structures. This feature is observed only for the M06 between those considered here. Therefore, taking into account all these factors, we have used for our purposes for the geometry optimizations the PBE functional, which additionally is computationally efficient; and for the energies we have employed the M06 functional. The same functional was also used in our previous work on magnesium (which displays similar, although less evident, problematic behavior) and magnesium hydride systems [9]. The M06 functional, on top of being quite accurate, also displays a very systematic and consistent behavior for both the bare and hydrogenated systems, and small and larger sizes. We find this attribute of M06 very appealing for the study of the specific systems. With the same criteria of consistency, and computational efficiency and economy for the systems studied here, an alternative second choice could have been the B97-D functional.

As was mentioned above, the geometry optimizations were performed without any symmetry constraints. A large number of initial geometries have been taken under consideration in an attempt to account for as many configurations as possible. After establishing an adequate population of energetically low-lying bare beryllium structures, we proceed in a stepwise hydrogenation process to produce the hydrogenated clusters by adding two hydrogen atoms at each step. For each bare cluster, the hydrogen atoms are positioned at various sites and the resulting hydrogenated structures are re-optimized. The additional hydrogenation and subsequent optimization procedure is repeated until the final hydrogen content of the clusters becomes double the number of beryllium atoms. Linear configurations are also included in the population of clusters with high hydrogen content. For the resulting energetically lowest clusters of each

step, vibrational analysis has been performed to determine the dynamical stability (i.e identify vibrational modes with imaginary frequencies) and to calculate the zero point energy (ZPE) of the structures.

Furthermore, all-electron ab initio molecular dynamics (AIMD) simulations were additionally performed for selective low-lying Be_nH_{2n} structures as a means to identify possible existing energetically lower nearby local minima conformations. The simulations were performed in the canonical and microcanonical ensemble, within the framework of DFT, employing the PBE functional and using the def-SVP basis set for computational economy. To further increase the computational efficiency, the two-electron integrals were treated using the resolution of the identity approximation [35]. The simulation duration was between 1 and 20 ps depending on system size, using a timestep of 0.97 fs, at an initial temperature of 1000 K. The Nosé-Hoover [36] thermostat was employed initially for a short time period. The procedure was followed by a simulated annealing with an annealing factor of 0.9–098 (over 100 timesteps) until temperatures below 700–800 K where reached. In this procedure, the energetically lowest structures, if any, would be picked out of the MD trajectories, followed by geometry optimization. Yet, even when no new energy minima could be found, as in our case, this procedure does not ensure that the global minimum structures were obtained. Clearly, this is not the objective of the present study, but it is only an additional test to ensure that no lower nearby local minima exist in the vicinity of structures we have already obtain as local minima. All of the AIMD calculations were performed using the Turbomole package [37].

In addition to the H desorption energies $\Delta E_{sd}(Be_nH_m)$ and $\Delta E_{ssd}(Be_nH_m)$ for BeH_2 clusters (and nanocrystals), we have systematically examined the binding energies or small and medium bare

13

Be$_n$ clusters and, in particular, large Be$_n$ nanocrystals. As will be shown in the next section, these results, properly extrapolated lead to the binding energy of crystalline Be metal.

3. Binding energy of Be$_n$ Nanocrystals

The structures of the small beryllium clusters are similar to the ones given in the literature [10, 14]. The optimized structures of the larger "crystalline" Be$_n$ nanocrystals, obtained here are given in Fig. 1. The initial geometries of these nanocrystals, contrary to the Be$_n$ (nano)clusters, were generated as spherical cuts from the bulk crystalline beryllium. As we can see in Fig.1, these structures are not completely spherical, neither fully symmetrical (with full point group symmetry of the bulk crystal), which would be expected in view of the unconstrained geometry optimization of the initial bulk fragments. Yet, they are quite compact and "regular" shaped, representing normal nanocrystals in equilibrium under "metallic" binding. The binding (or atomization) energy E$_b$ of a Be$_n$ nanoparticle was given before in (3.a). The binding energy per atom ($E_b(\mathrm{Be}_n)/n = [nE(\mathrm{Be}) - E(\mathrm{Be}_n)]/n$) of all (small, medium and large) Be$_n$ nanoparticles is plotted in Fig. 2. The calculated points (shown in solid squares) from n =2 up to n=166 with M06 functional have been fitted to the smooth curve of the figure, which has the general form [9] :

$$B.E.(\mathrm{Be}_n) \equiv y = A + B \cdot (x \equiv n)^m \qquad (6).$$

The fitted parameters include the constants A , B and the exponent m, which was left free to vary, since in our fit we have included all nanoclusters (lowest energy free clusters) and nanocrystals (constructed as near-spherical cuts from the bulk crystal) of all sizes and symmetries from n=2 to n=166. For perfectly spherical and symmetrical nanocrystalls we would have expected m=-0.333 [9]. Here we have obtained m= -0.54±0.04, which is very reasonable in the present case. The value of the constant A is very crucial and important, since as we can see

14

from the form of eq. (6), it represents the value of the binding energy in the limit n→∞, e.g. the binding energy of the bulk crystal. Unexpectedly enough, we have obtained here the value A=(314.1±6.6) kJ/mol, or (3.26±0.06) eV per atom; Whereas, the experimental binding energy is [18]: 320 kJ/mol or 3.32 eV per atom.
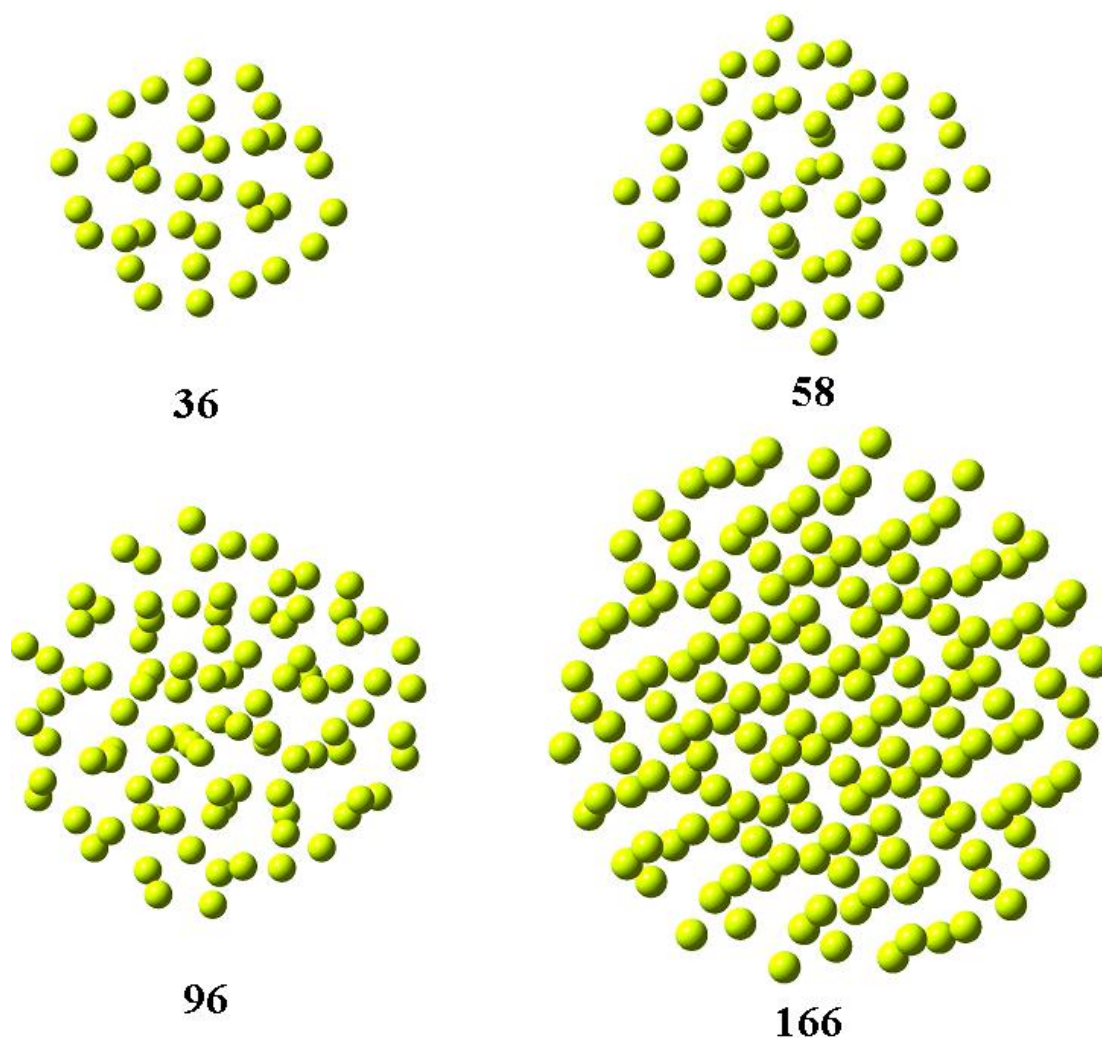
FIGURE 1. The structure of the large Be_n (n= 36, 58, 96, 166) nanocrystals.

This type of agreement (± 6.6 kJ/mol $\approx \pm 1.6$ kcal/mol $\approx \pm 0.06$ eV) is unbelievably good, especially if one considers: 1) the simplicity of the method, and 2) the fact that earlier (sophisticated) full band-structure methods for the Be crystalline solid [18] have obtained binding energy values from 3.60 eV to 3.70 eV per atom (see table 1 in ref 18).
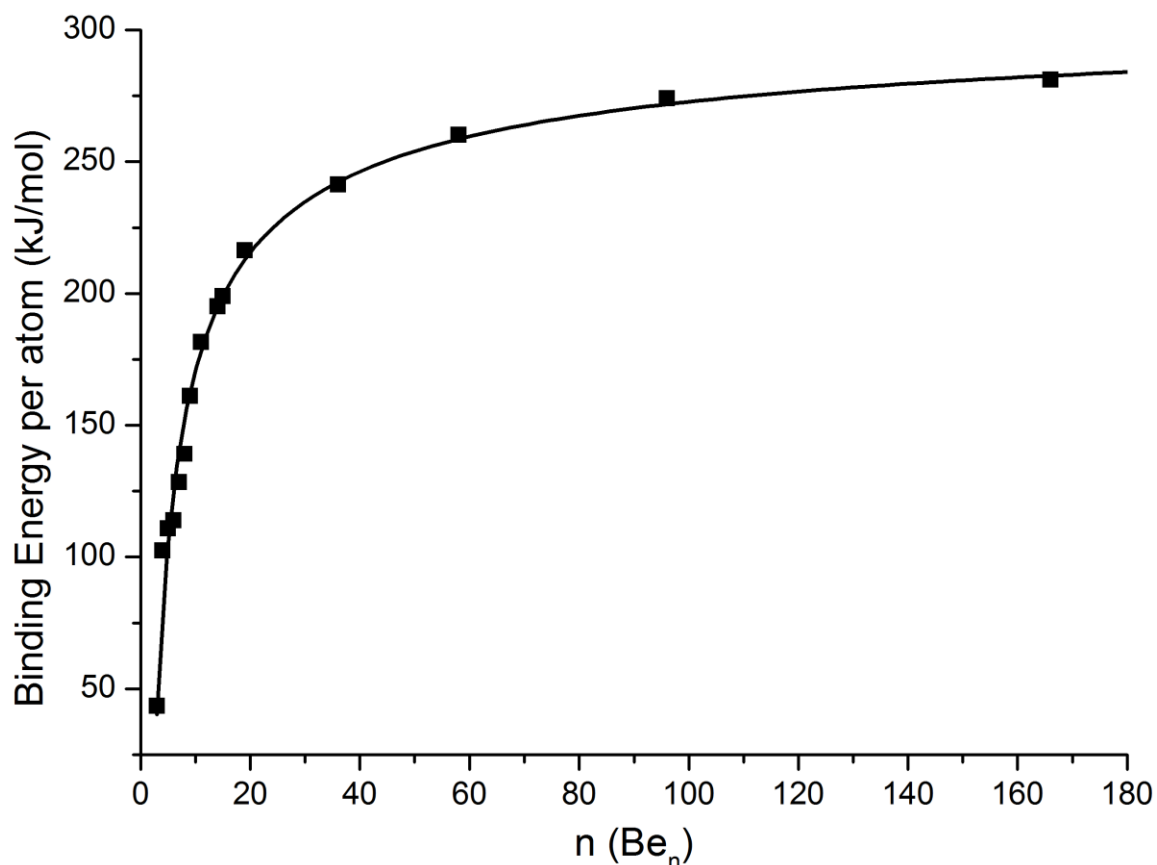
FIGURE 2.   Binding energy per atom of Be_n nanoparticles in kJ/mol. Full squares denote calculated results. Solid line corresponds to the fit of eq. (6).

It could be certainly claimed that this type of agreement is rather fortuitous. However, we strongly believe that the success of this relatively simple method is based on: (a) the proper selection of the M06 meta-functional, and (b) the appropriate selection and optimization of the lowest energy structures for the nanoclusters, and the original (before optimization) bulk

16

fragments for the nanocrystals, so that they will be representative of the crystalline environment. This will be further illustrated below for the predicted binding energy of $[BeH_2]_\infty$ chains, where we use exactly the same technique.

Obviously, analogous conclusions hold for the calculation of desorption energies.

4. Desorption Energy of Small and Medium size Be_nH_m Nanoparticles

4.1 Small Be_nH_m Nanoparticles

Following the process outlined in section 2, we have obtained and fully optimized the structures of small (n<8) Be_nH_{nx} nanoparticles for various concentrations (m=nx) of hydrogen, similarly to our earlier work for Mg_nH_m nanoparticles of analogous size [9]. Representative equilibrium structures for such nanoparticles are shown in Fig. 3. As we can see in Fig. 3, although for small values of x (x≤1) the Be_nH_{nx} structures are not much different from the corresponding Mg_nH_m structures, for larger values of x, we have completely different results compared to Mg_nH_{nx}. We can see first the formation of ring structures (for x<2), and finally at the stoichiometric value x=2 we have linear chains as the most stable structures. This is in agreement with the results in refs. 10 and 14. Most of the hydrogenated nanoclusters are highly symmetric. For example, Be_5H_2 has D_{2h}, Be_4H_2 and Be_4H_4 have D_{2d}, Be_4H_6 has T_d, and Be_3H_2 has C_{2v}. The Be_nH_{2n} chains are of either D_{2h} or D_{2d} symmetry. Hydrogen atoms more commonly prefer locations between two Be atoms but they may be also found between three Be atoms and less often close to one Be atom. The Be_nH_m nanoclusters normally can hold up to $m=2n$ hydrogen atoms. Increasing the number of hydrogen above 2n (x>2), results to structures with the additional hydrogen atoms located away from the nanocluster, forming hydrogen molecules. However, in some cases of linear chains configurations the structure can retain up to four additional hydrogen atoms, two on each

edge, without the formation of molecular hydrogen. The calculated normalized and stepwise desorption energies desorption energies, given in eqs. (4) and (5), are shown in Figs. 4(a) and 4(b) respectively.
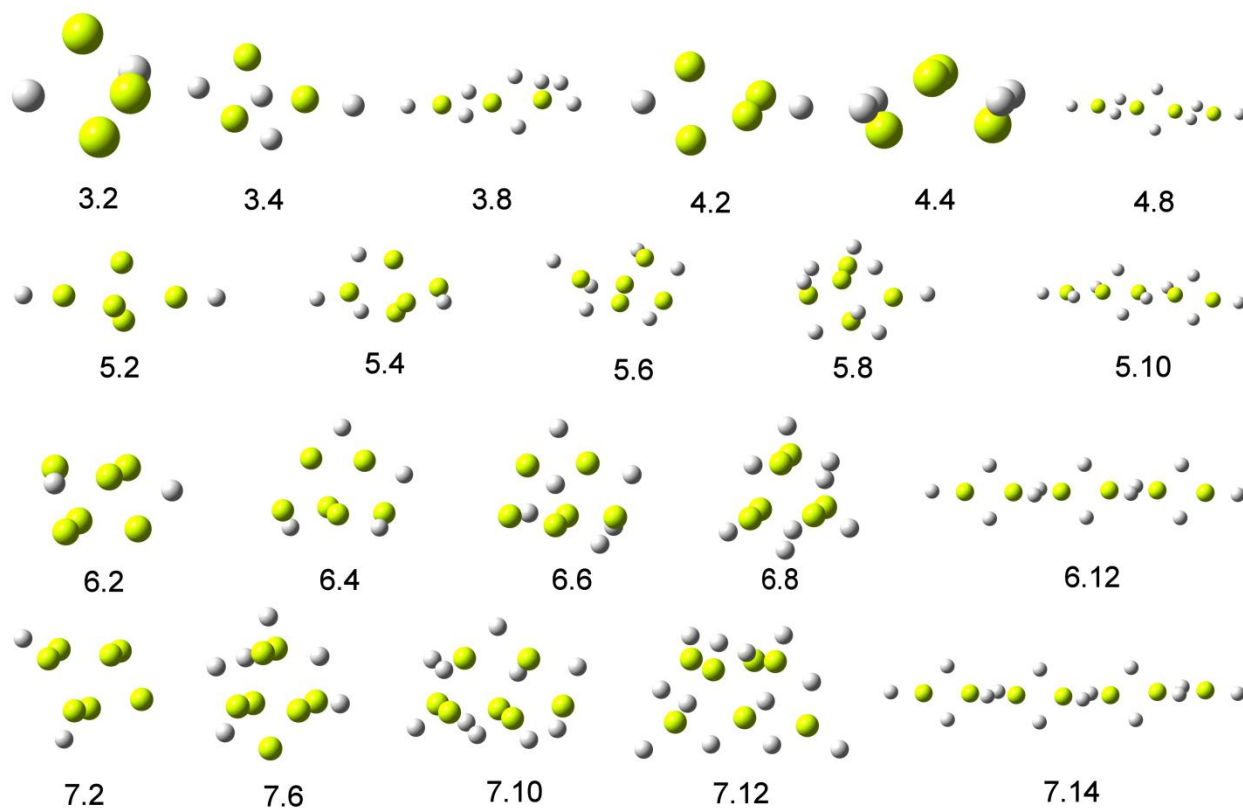
**FIGURE 3.** Equilibrium geometries for representative Be_nH_m, $n=3–7$, $m=2–14$, nanoparticles.

There is a general trend of the normalized desorption energy in Fig. 4(a). For each n, ΔE_d starts from its highest value for small x ($x\approx0.2$-0.4) and slowly drops as x increases until it reaches a low value for x=2. For x>2 there is a similar drop in ΔE_d which continues until the structure completely destabilizes. This universal behavior is a direct result of the formation of molecular hydrogen in the direct vicinity of the cluster upon an increase of the hydrogen content x above the value x=2. This additional hydrogen molecule is weakly bound to the Be_nH_{2n} cluster. The

only exception to the trend of decreasing ΔE_d as x increases up to the value of 2 is for the $n=3$

clusters, in which case the desorption energy actually increases as x increases (up to x=2).
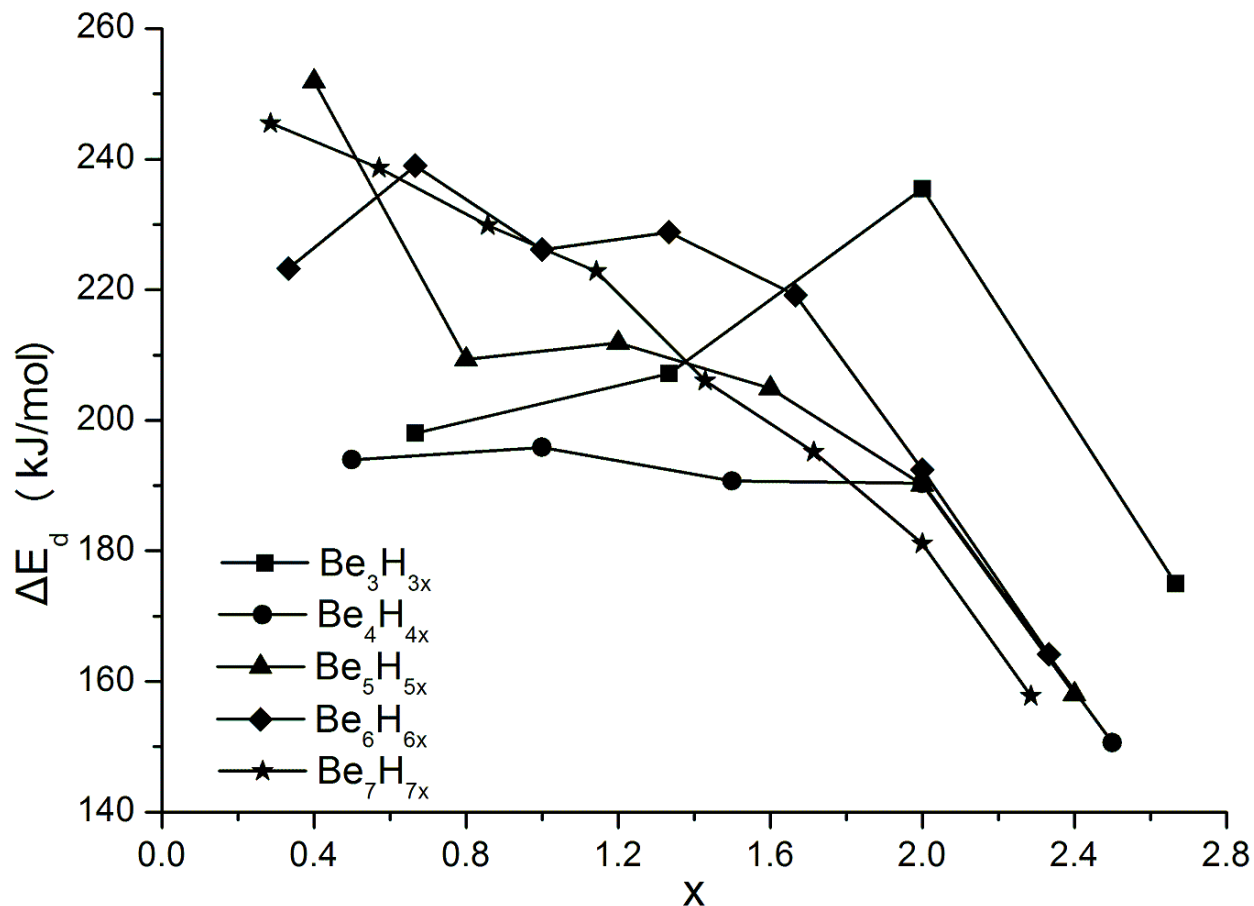
FIGURE 4(a). Normalized Desorption Energy $\Delta E_d(Be_nH_m)$, in kJ/mol, for representative

Be_nH_m $n=3-7$, $m=2-16$ obtained at the DFT/M06 level of theory.

The $n=4$ series of clusters seems to have the slowest drop of desorption as x (m) increases. The

highest normalized desorption energy is 250 kJ/mol for Be_5H_2 while the smallest one (excluding

the x>2 cases) is 180 kJ/mol for the Be_7H_{14} cluster. The stepwise desorption energies, as we can

see in Fig. 4(b), follow a similar trend (reduction in desorption energy as x increases).
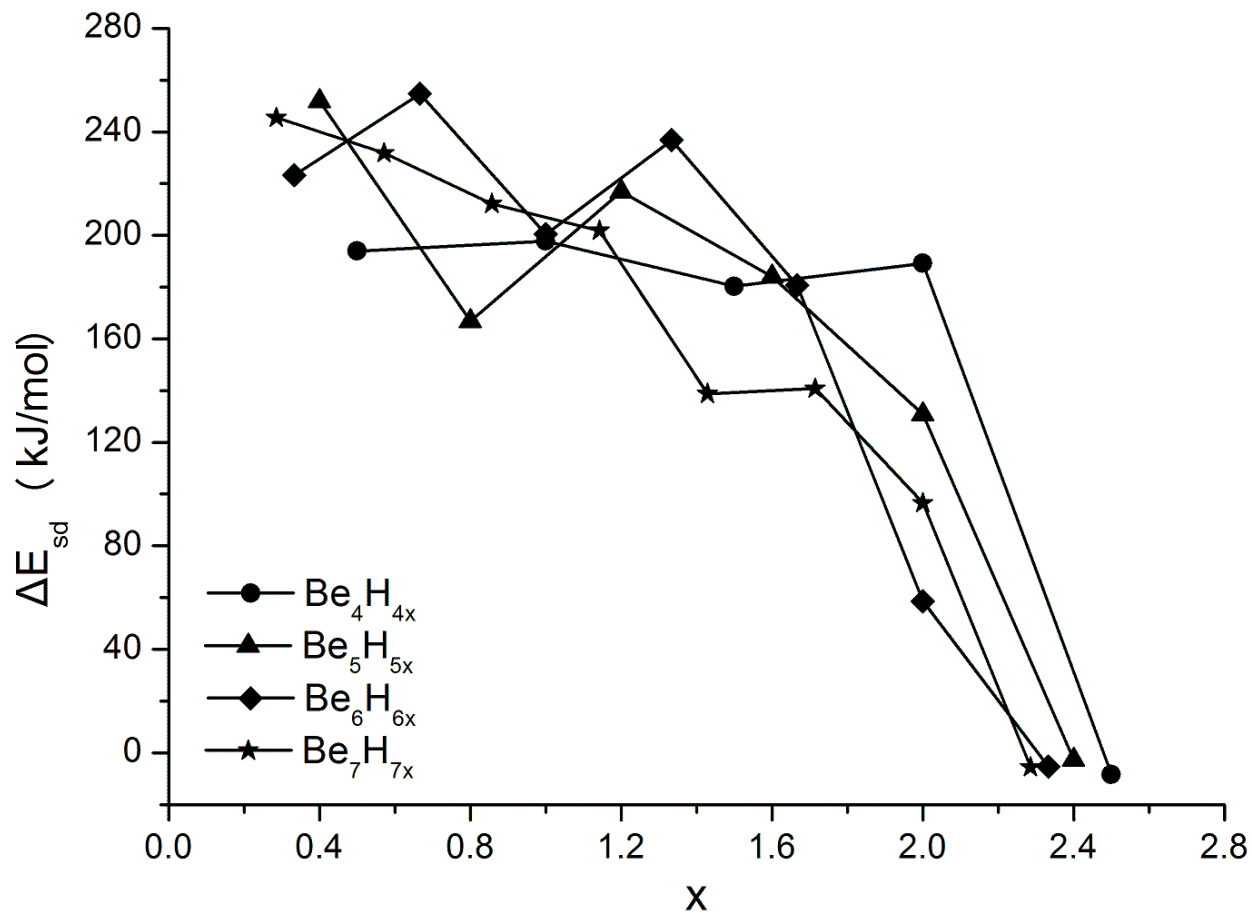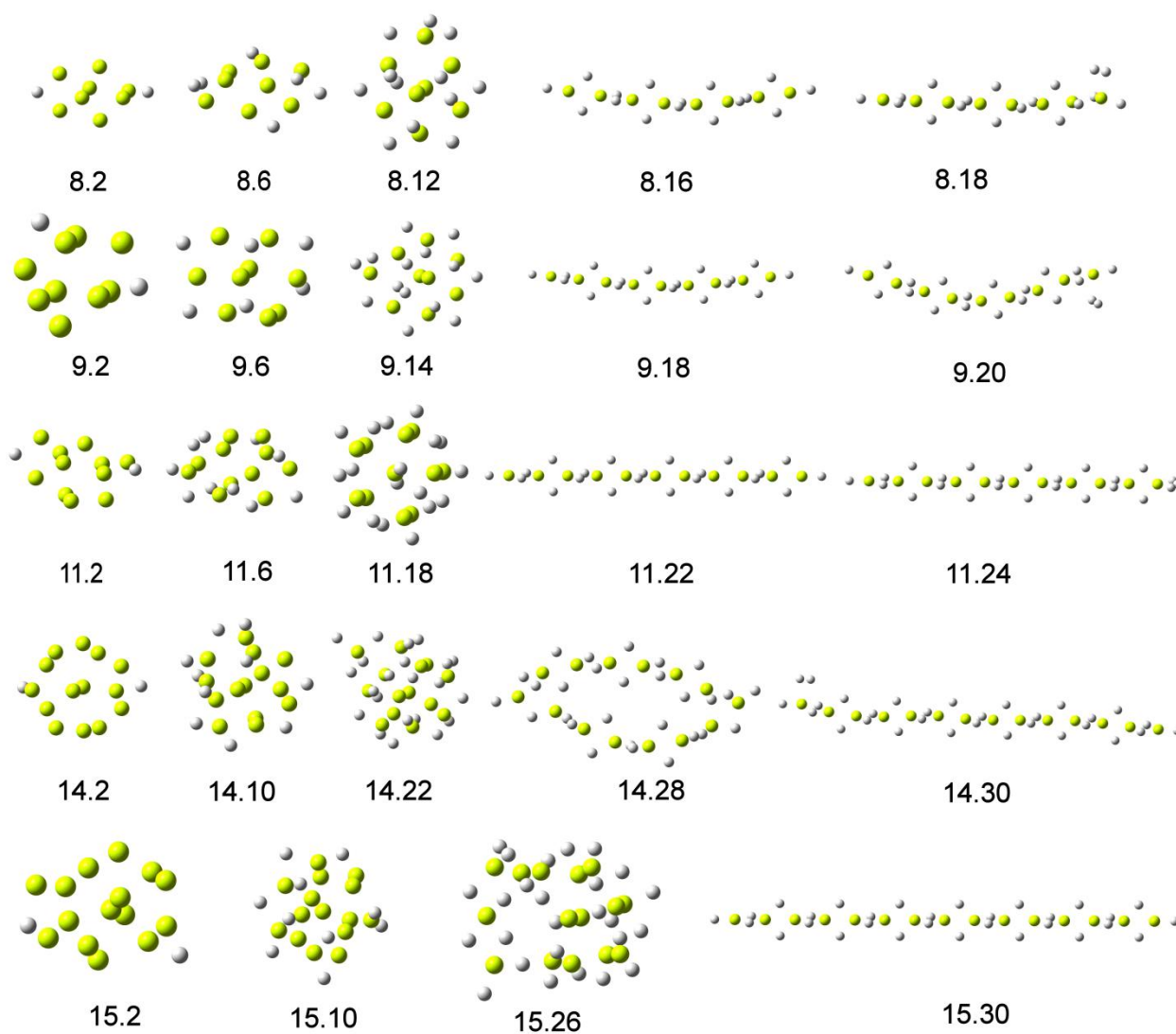
FIGURE 4(b). Stepwise Desorption Energy $\Delta E_{sd}(Be_nH_m)$, in kJ/mol, for representative Be_nH_m, n=4–7, m=2–16 clusters, obtained at the DFT/M06 level of theory.

4.2 Medium size Be$_n$H$_m$ Nanoparticles

Some representative medium size Be_nH_m clusters ($8\leq$ n $\leq$19) are shown in Fig. 5. Excluding the

Be_nH_{2n} cases, most of these clusters have no symmetry with the exception of Be_8H_2 with D_{2d},

and some other clusters with C_s symmetry (Be_9H_2, Be_9H_{10}, $Be_{11}H_{14}$, $Be_{14}H_2$, $Be_{14}H_{22}$, and $Be_{15}H_2$). As we can see in Fig. 5, the structural trend towards chain formation for x ≈2 described above for the small clusters, holds also true for the medium-size clusters. We can see that in the case of n=14, m=28 (x=2), the ring structure is slightly more stable than the corresponding chain, which again is the lowest energy structure for slightly higher value of x, at m=30.

| 8.2 | 8.6 | 8.12 | 8.16 | 8.18 |

| 9.2 | 9.6 | 9.14 | 9.18 | 9.20 |

| 11.2 | 11.6 | 11.18 | 11.22 | 11.24 |

| 14.2 | 14.10 | 14.22 | 14.28 | 14.30 |

| 15.2 | 15.10 | 15.26 | 15.30 |

FIGURE 5. Representative lowest energy structures of medium Be_nH_m, n=8, 9, 11, 14, 15, (m = 2-30) clusters.

We can also observe, both in Fig. 3 and Fig5, that in most of the Be_nH_{xn} structures the hydrogen atoms are more or less at the surface of the nanoparticles, contrary to Mg_nH_{xn} nanoparticles (and especially when x approaches 2) where a significant number of hydrogen atoms is inside the nanoparticles [9]. The desorption energies of the medium-size Be_nH_m clusters are shown in Figs. 6(a), (for n=8, 9, 11, 14) and 6(b) for n=15, 19. As in the small size clusters, the desorption energies in each Be_nH_m cluster, decrease as m (x) increases towards m=2n (x=2). A notable exception to this rule, as we can see in Fig. 6(a), is the $Be_{11}H_{14}$ (x≈ 1.3) case which exhibits a peak in the desorption energy (at x≈ 1.3). This could be due to of higher (C_s) symmetry, compared to C_1 for the rest $Be_{11}H_{11x}$ structures.
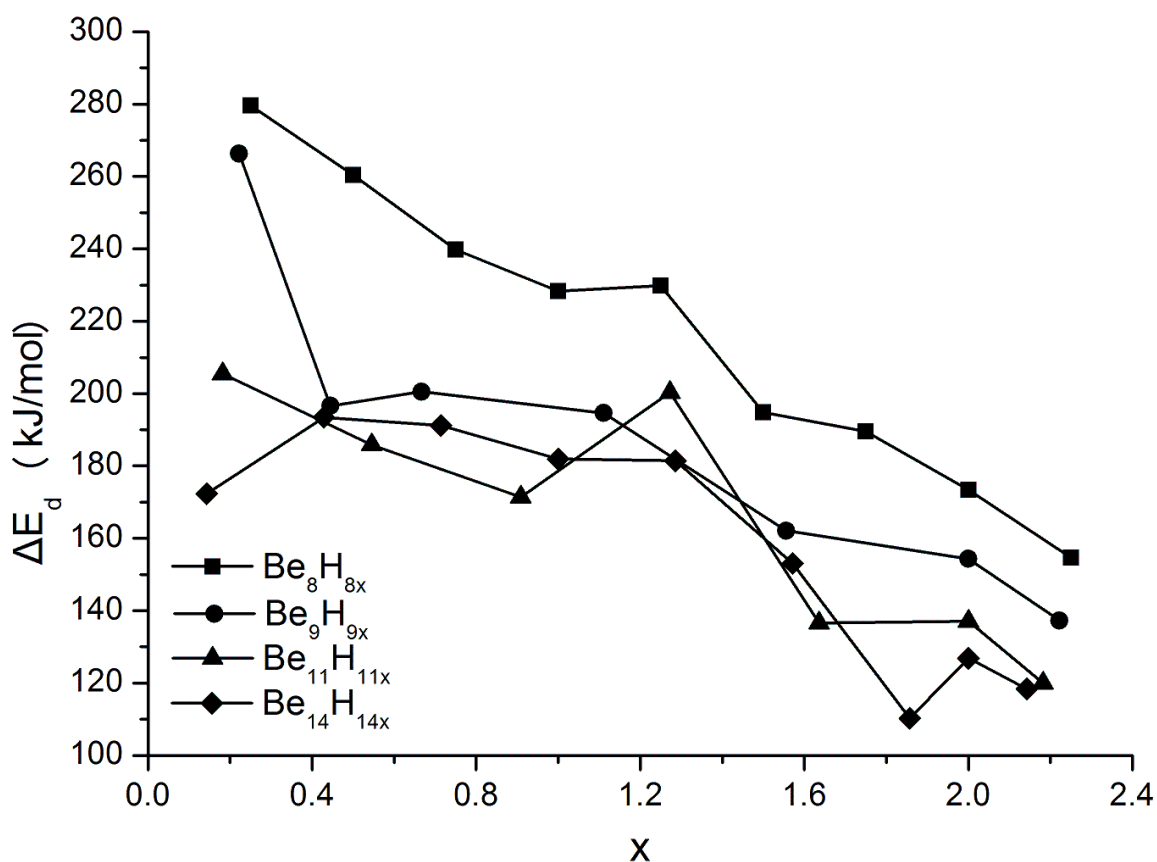
FIGURE 6(a). Normalized Desorption Energy $\Delta E_d(Be_nH_m)$, in kJ/mol, for several medium size Be_nH_m clusters ($n=8–14$)

The highest desorption energy is 280 kJ/mol for the Be_8H_2 cluster. The lowest is around 103 kJ/mol for $Be_{19}H_{40}$, followed by $Be_{19}H_{38}$ (≈ 108 kJ/mol), and $Be_{14}H_{26}$. (110 kJ/mol). As we can see in Fig. 6, almost in all cases (with best example $Be_{19}H_{40}$), there is a general trend of lower desorption energies in the oversaturated hydrogen range of concentrations ($x \geq \approx 2$), which is common to all (small, medium, and large) Be_nH_{xn} and other, such as Mg_nH_{xn} [9], metal hydride nanoparticles.

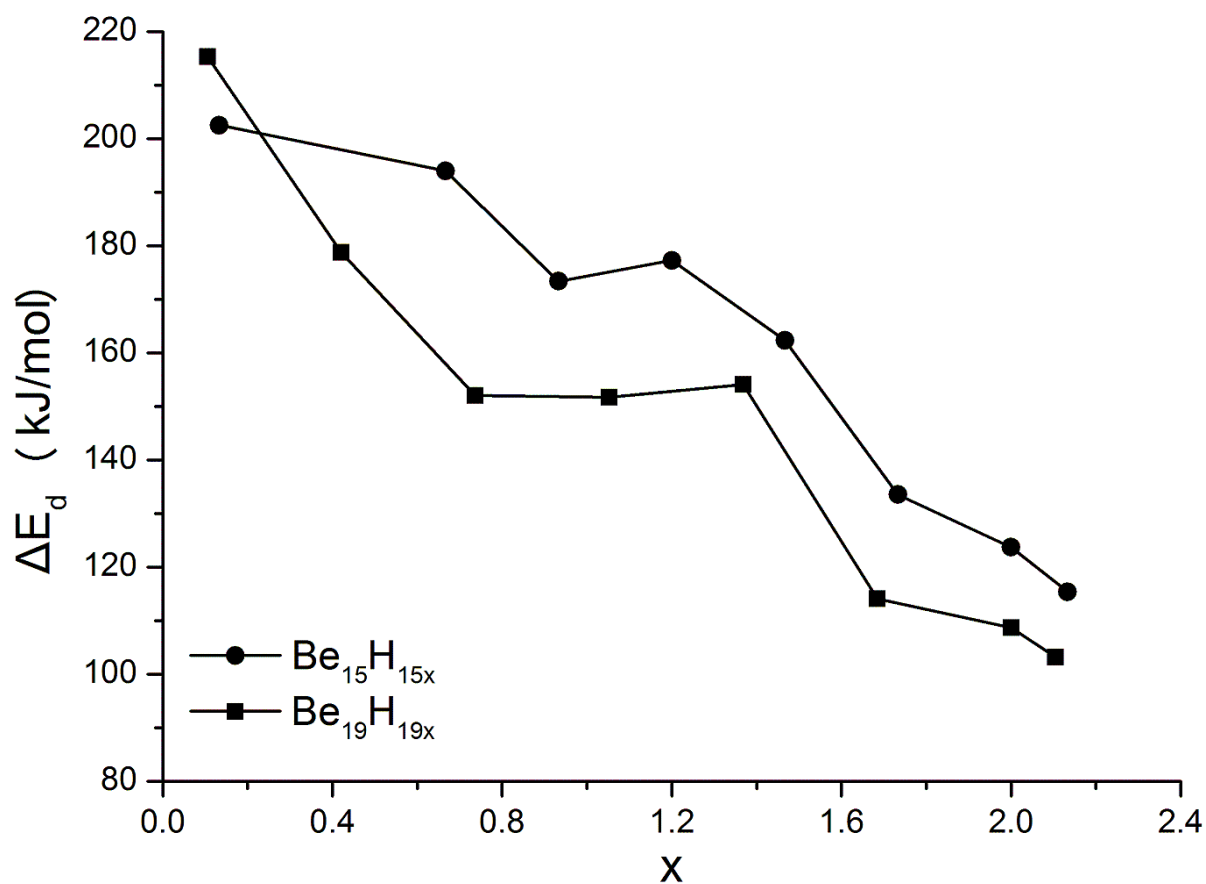**FIGURE 6(β)** Desorption Energy $\Delta E_d(Be_nH_m)$, in kJ/mol, for the Be_nH_m clusters with n=15, 19.

5. Large Stoichiometric [BeH$_2$]$_n$ Nano-clusters, and Nano-crystals, and Nano-chains.

5.1 Nanoclusters and Nanocrystals Some representative large-size low-energy [BeH$_2$]$_n$ nanoparticles are shown in Fig. 7.
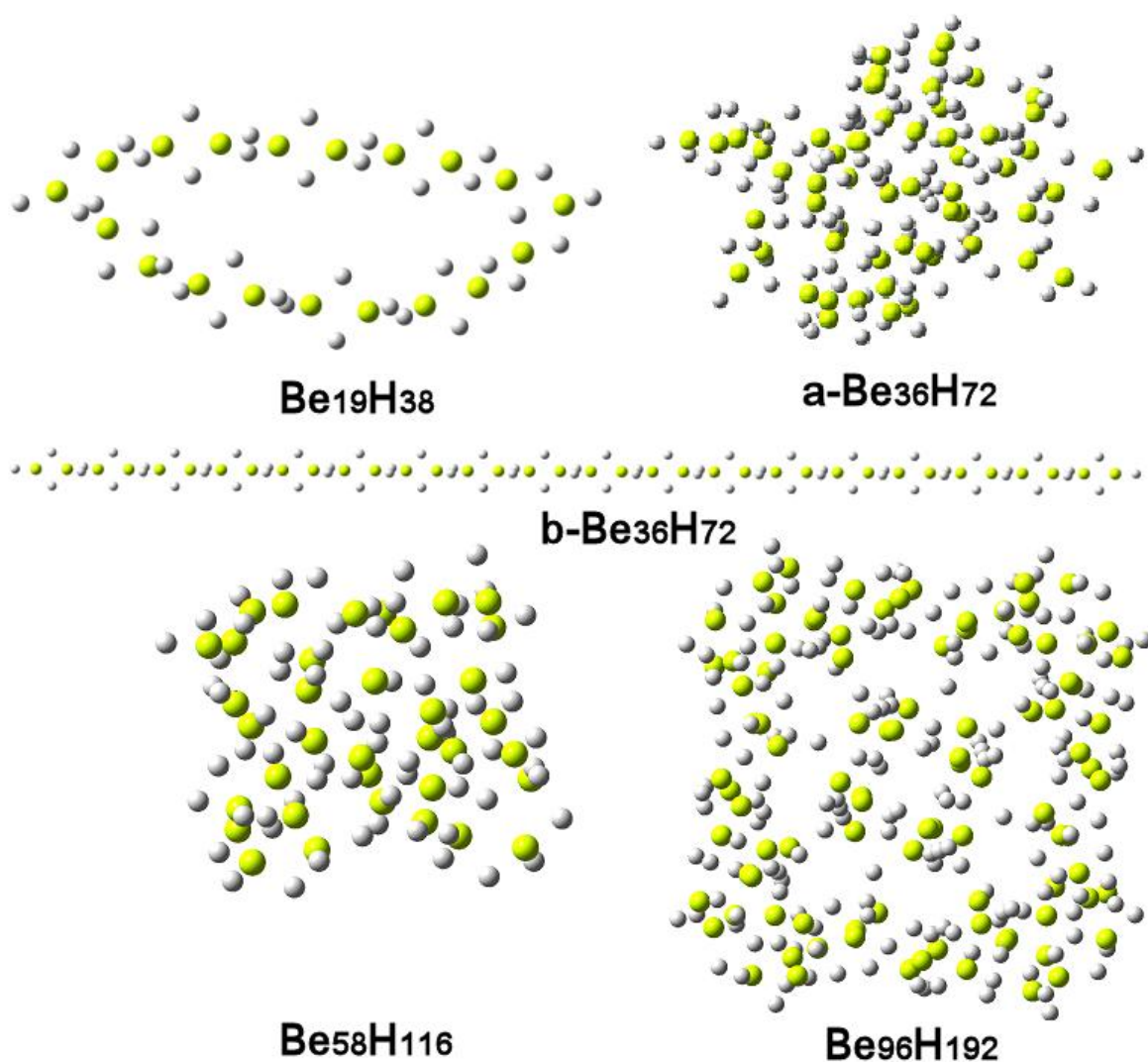

FIGURE 7. Representative large-size low-energy Be_nH_{2n} structures (n=19, 36, 58, 96).

As we can see, Fig. 7 includes some representative but very diverse structures, among which rings, chains and distorted "bulk-like" fragments. The origin of these structures is also different. The structure of $Be_{19}H_{38}$ was generated through the standard procedure (of successive hydrogenations) described in section 2, and it is one of the few cases (if not the only one) in which the ring structure is more stable than the chain structure. Thus, as we can also see in Figs. 3 and 5, all stoichiometric nanoclusters we have considered, with the exception of $Be_{19}H_{38}$, are chains. The linear chain structure b-$Be_{36}H_{72}$ in Fig. 7, which will be discussed separately in section 5.2 below, was constructed from the beginning as such with alternating H-bridging bonds and was further optimized.

The remaining three structures in Fig. 7, were constructed as much as possible as "spherical cuts" from the bulk crystal structure, which subsequently were appropriately truncated to preserve the required stoichiometry $[BeH_2]_n$. This, most of the times, is accomplished at the expense of proper symmetry and proper bonding. Certainly the following up unconstrained geometry optimization can alleviate some of the problems but not all of them, and not always. The case of $[BeH_2]_n$ is one of the most difficult for such a treatment because of its geometrical and electronic structure. The structure of BeH_2 is body-centered orthorhombic with 12 BeH_2 formula units per conventional cell. It consists of an array of corner-sharing BeH_4 tetrahedral linked by H atoms, and there is no known analogue among other compounds containing tetrahedral building blocks. Moreover, while all the binary alkaline earth hydrides are insulators, BeH_2 is unique in that it is the only covalent hydride, as opposed to ionic bond character. Thus, contrary to MgH_2, not only it is difficult to properly "cut the nanocrystal from the bulk", but is even more difficult to avoid "dangling bonds" and have a proper binding. As a result, the a-$Be_{36}H_{72}$ nanocrystal in Fig. 7 is less stable than the corresponding b-$Be_{36}H_{72}$ nanochain (in the

same Figure) by about 14 kJ/mol. The same is true for the other two nanocrystals (originated as "bulk cuts"), as we can see in Table 2, which lists the corresponding binding energy per formula unit:

$$E_b\{[BeH_2]_n\}/n = \{nE(Be) + 2nE(H) - E[BeH_2]_n\}/n \quad (\mathbf{7}).$$

TABLE 2. Binding energies per formula unit, $E_b\{[BeH_2]_n\}/n$, of $[BeH_2]_n$ nanoparticles (n=36, 58, 96) in kJ/mol, at the DFT/M06 level of theory, with the cc-PVTZ basis set.

Particle	E_b (kJ mol^{-1})	E_b (kJ mol^{-1})	ΔE_b (kJ mol^{-1})
	Chain	Nanocrystal	
$Be_{36}H_{72}$	753.6	739.3	14.3
$Be_{58}H_{116}$	755.6	746.3	9.3
$Be_{96}H_{192}$	755.6	748.6	7.0

Thus, almost all stoichiometric nanoclusters and nanocrystals examined here have lower binding energies from their chain isomers. This is because the chains are by construction fully and correctly bonded with alternating H-bridge bonds (without any dangling or otherwise unfavorable bonds) and fully optimized. If one was going to assume that this trend continuous all the way to very large nanoparticles (n→∞), the results in Table 2, if taken at face value, seem to suggest that the polymeric structure, once believed to be the real structure of solid BeH$_2$ [38–39], is indeed the lowest energy structure, at least at 0 °K. This is not so strange as it appears to be , if one considers that in the early years of BeH$_2$ synthesis [38], the products were almost invariably amorphous polymeric solids containing BeHHBe chains [see references 37, 38 and references therein]. We should notice however, that the differences in E$_b$/n become smaller as size

increases, apparently due to the decrease of the surface to volume ratio; and therefore one could assume that, at some much larger size, such differences will become zero and eventually negative. This remains to be seen, especially if one observes in Table 2 that the nano-chain binding energies seem to have already reached saturation values. Nevertheless, in either case, we are lead to examine the binding and desorption energies of the nano-chains, which with their well- defined structural and bonding properties have emerged as reference points for each size of nanoclusters and nanocrystals (all the way to n→∞). The corresponding desorption energies for the nanoparticles of Table 2 are given in Table 3. Obviously, from the definitions of desorption and binding energies, eqs. (1)-(3), the differences would be the same. Due to their lower stability, the nanocrystals clearly would have lower desorption energies.

TABLE   3. Desorption energies (ΔE_d) in kJ/mol for the $Be_{36}H_{72}$, $Be_{58}H_{116}$, and $Be_{96}H_{192}$ nanocrystals and nanochains at the M06/ cc-PVTZ level of theory.

Particle	ΔE_d (kJ mol^{-1}) Chain	ΔE_d (kJ mol^{-1}) "Crystal"	$\Delta(\Delta E_d)$ (kJ mol^{-1})
$Be_{36}H_{72}$	79.1	64.8	14.3
$Be_{58}H_{116}$	61.7	52.4	9.3
$Be_{96}H_{192}$	57.3	50.3	7.0

5.2 [BeH$_2$]$_n$ Nano-chains.

From the discussion above, it is clear that we should approach the binding and desorption energies of Solid BeH$_2$, indirectly, through (with reference to) the binding and desorption energies of infinite [BeH$_2$]$_n$, n→∞, chains, which model the polymeric form, initially thought off as the equilibrium crystal structure of solid beryllium hydride. The binding energies per formula

unit of the various $[BeH_2]_n$ chains from Figs. 3, 5, and 7 (and more) have been plotted in Fig. 9. as a function of size n. All these chains are dynamically stable (no imaginary frequencies) and well converged. The solid line has been obtained by a fit to relation 6, with free parameters the constants A, B, and the exponent m. From this high quality fit, as we can see in Fig. 9, we can obtain the asymptotic binding energy of the infinite polymeric chain, through the constant A, which is equal to 757.81 kJ/mol (±0.2 kJ/mol) or 7.85 eV (±0.02 eV).
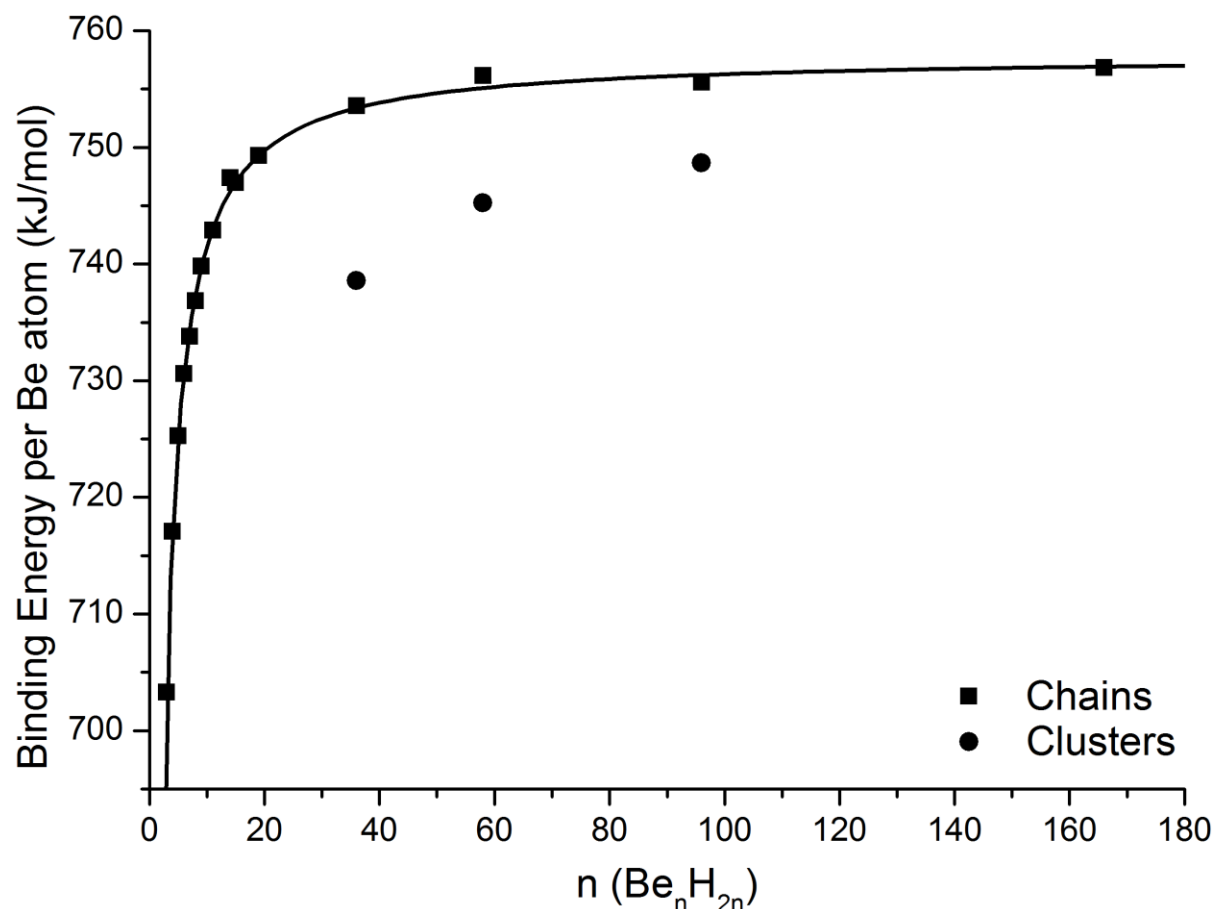
FIGURE 8. Binding energy, $E_b\{[BeH_2]_n\}/n$, of $[BeH_2]_n$ nanochains (solid squares). Isolated results for $[BeH_2]_n$ nanocrystals are presented by solid circles. The fitted solid line is discussed in the text.

This is the predicted value of the present calculation. Another important finding is the value of the exponent m (which was free to vary in the fit). We have obtained from the fit the value: m=-1.03±0.03, in other words the absolute value of m is equal 1 (m=-1/1), instead of an expected value of -1/3 for a homogeneous 3-dimensional solid [9]. This is in perfect agreement with the 1-dimensional nature of the chains. The error bars for the binding energy (constant A in eq. 6) and for the exponent are the statistical errors of the fit, which is of excellent quality. This verifies a posteriori the essential correctness of the present extrapolating method. However, we can not say very much for the binding energy of the real orthorhombic BeH_2, except perhaps that it would be expected to be "quite close" around the value of 757.8 kJ/mol, but not necessarily lower or higher, although a calculation of desorption energy could possibly give as an indirect hint. To this end, we examine the implications on the corresponding desorption energies. The desorption energies versus size (n) of the polymeric chains are shown in Fig.9.
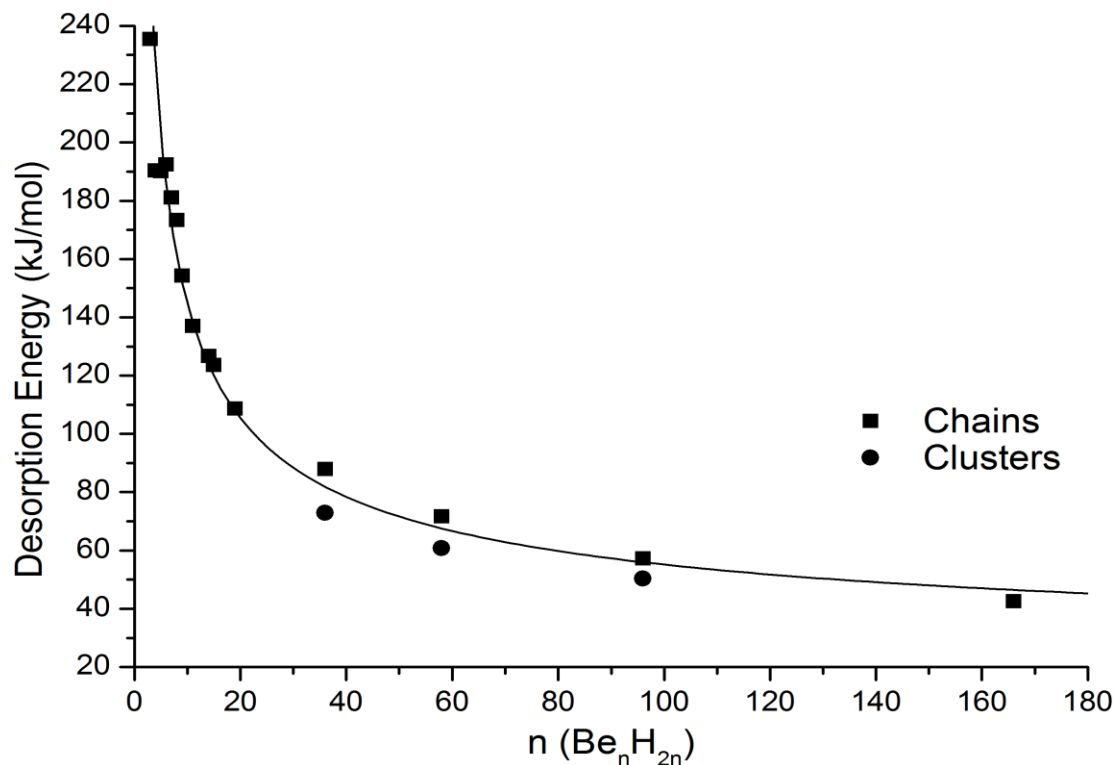
FIGURE 9. Desorption energy ΔE_d of Be_nH_{2n} nanochains (solid squares). Isolated results for $[BeH_2]_n$ nanocrystals are presented by solid circles. The fitted solid line is discussed in the text.

The connection between desorption, $\Delta E_d(Be_nH_{2n})$, and binding energies per formula unit, Be_nH_{2n}, of $E_b(Be_nH_{2n})$ from the definitions (2) and (7) is given as:

$$\Delta E_d(Be_nH_{2n}) = [E_b(Be_nH_{2n}) - E_b(Be_n)]/n - E_b(H_2) \quad (7) .$$

Therefore, it would be reasonable to fit the calculated desorption energies, shown in solid squares in Fig. 9, to a form like $\Delta E_d\{[BeH_2]_n\} = A + B \cdot (n)^{-1} + C \cdot (n)^{-0.54}$ $\quad$ (8), which combines the $(n)^{-1}$ and the $(n)^{-0.54}$ variation of the binding energies of the $[BeH_2]_n$ nanochains and Be_n nanocrystals respectively. Such a fit, however, is not practically acceptable because it yields unrealistically large uncertainties to the value of A (2.58±3.59) which is the key quantity of interest. Since at large sizes (n) the desorption is dominated by the longest-range term $C \cdot (n)^{-0.54}$, we have chosen to fit the calculated desorption energies (using a size weighted fit) to the simple $\Delta E_d\{[BeH_2]_n\} = A + C \cdot (n)^{-0.54}$ form. The value of A obtained this way is A=18.88±2.66 kJ/mol, which is unbelievably close to the experimental value of 19 kJ/mol for solid BeH_2 at room temperature. Although this could be considered as fortuitous, it is (even in that case) highly suggestive of the essential correctness of our present approach. Furthermore, the very close proximity of the desorption energy values implies a similarly close proximity in the corresponding binding energies of the polymeric and rhombic forms of solid BeH_2, which is in full accord with the early difficulties and discrepancies in determining its real crystal structure.

6. Conclusions

Employing the judiciously chosen M06 meta-functional, after comparison(s) with high level coupled clusters, CCSD and CCSD(T), *ab initio* calculations, we have performed an extensive study of the structural and cohesive properties of Be_n, Be_nH_m, and $[BeH_2]_n$, nanoparticles, as a function of both n and m (n=2-166, m =n- 2n+2, in most of the cases).

Using these primary results we have calculated: 1st) the binding and desorption energies of these nanoparticles as a function of size (n) and composition (x), and 2nd) the corresponding binding and desorption energies of the infinite systems, by a carefully selected extrapolation scheme.

In the first case, we have found that:

(a) the majority of the lowest energy structures of stoichiometric Be_nH_{2n} nanoclusters are chains or chain-like structures. The tendency towards chain stabilization of Be_nH_{xn} nanoparticles increases, as x approaches the stoichiometric value x=2.

(b) Contrary to Mg_nH_{xn} [9], for a given size (n), generally the desorption energy as a function of hydrogen content decreases almost monotonically with increasing x up to the stoichiometric limit x=2 (m=2n), without the characteristic dip of Mg_nH_{xn}, at sub-stoichiometric concentrations. In very few cases, we can have relatively stable Be_nH_{xn}, structures for m=2n+2. In these over-stoichiometric cases the behavior is similar to Mg_nH_{xn} (decreasing ΔE_d , formation of H_2 molecules near the surface) nanoparticles.

In the second type of calculations we have sensibly extrapolated the results for Be_n and $[BeH_2]_n$ stoichiometric nanocrystals and nanochains as n→∞ to find in very good agreement with experiment:

31

(c) The binding energy of crystalline Be has been obtained with very good agreement with experiment. This is particularly important in view of the much larger error of other "higher level" methods.

(d) For the polymeric forms of bulk BeH_2, which in the past have been considered as the leading forms of solid BeH_2 we have found that, as was anticipated that the binding energy varies exactly proportionally to n^{-1} leading to a predicted binding energy for $[BeH_2]_\infty$ of 7.85 eV, with expected accuracy of ± 0.02 eV.

(e) The extrapolated desorption energy for such polymeric forms of solid BeH_2 is found to be 19 ± 3 kJ/mol, which is almost identical to the experimental value of 19 kJ/mol for solid BeH_2.

(f) This small difference ΔE in cohesive energy between the orthorhombic and polymeric forms ($\Delta E \approx 3$ kJ/mol) is in full accord with the early (experimental and theoretical) discrepancies in determining and distinguishing the real crystal structure of solid BeH_2.

ACNOWLEDGMENTS

References

1. S. G. Chalk, and J. F. Miller, "Key challenges and recent progress in batteries, fuel cells, and hydrogen storage for clean energy systems", *J. Power Sources* **159**, 73 (2006).

2. B. Sakintuna, F. Lamari-Darkrim, and M. Hirscher, "Metal hydride materials for solid hydrogen storage: a review", *Int. J. Hydr. Energy* **32**, 1121 (2007).

3. U. Eberle, G. Arnold, R. von Helmolt, "Hydrogen storage in metal hydrogen systems and their derivatives", *J. Power Sources* **154**, 456 (2006).

4. S. Orimo, et. al., "Complex hydrides for hydrogen storage'', *Chem. Rev.* **107**, 4111 (2007).

5. M. T. Kelly, "Perspective on the storage of hydrogen: Past and Future", *Struct. Bond* **141**, 169 (2011).

6. H. Wu, "Strategies for the improvement of the hydrogen storage properties of metal hydride materials", *ChemPhysChem* **9**, 2157 (2008).

7. M. Fichtner, "Properties of nanoscale metal hydrides", *Nanotechn.* **20**, 204009 (2009).

8. V. Berube, G. Radtke, M. Dresselhaus, and G. Chen, "Size effects on the hydrogen storage properties of nanostructured metal hydrides: a review", *Int. J. Energy Res.* **31**, 637 (2007).

9. E. N. Koukaras, A. D. Zdetsis, M. M. Sigalas, "Ab initio study of Magnesium and Magnesium hydride nanoclusters and nanocrystals: Examining optimal structures and compositions for efficient hydrogen storage", *J. Am. Chem. Soc.* **134**, 15914–15922 (2012).

10. X. Wang and L. Andrews, "One-Dimensional BeH_2 Polymers: Infrared Spectra and Theoretical Calculations", Inorg. Chem. 2005, 44, 610-614

11. J. Wang, G. Wang, J. Zhao, "Density functional study of beryllium clusters with gradient correction", *J. Phys.: Condens. Matter* **13**, L753 (2001).

12. M. C. Heaven, J. M. Merritt, and V. E. Bondybey, "Bonding in beryllium clusters", *Annu. Rev. Phys. Chem.* **62**, 375 (2011).

13. C. W. Bauschlicher, D. H. Liskow, C. F. Bender, and H. F. Schaefer III, "Model studies of chemisorption. Interaction between atomic hydrogen and beryllium clusters", *J. Chem. Phys.* **62**, 4815 (1975).

14. Ch. B. Lingam, K. R. Babu, S. P. Tewari, and G. Vaitheeswaran, "Quantum chemical studies on beryllium hydride oligomers", *Comp. Theor. Chem.* **963**, 371-377 (2011).

15. F. Dong, Y. Xie, and E. R. Bernstein, "Experimental and theoretical studies of neutral $Mg_mC_nH_x$ and $Be_mC_nH_x$ clusters", *J. Chem. Phys.* **135**, 054307 (2011).

16. G. S. Smith, Q. C. Johnson, D. K. Smith, and D. E. Cox, "The crystal and molecular structure of beryllium hydride", *Solid State Commun.* **67**, 491 (1988).

17. M. G. Ganchenkova, V. A. Borodin, and R. M. Nieminen, "Hydrogen in beryllium: Solubility, transport, and trapping", *Phys. Rev. B* **79**, 134101 (2009).

18. A. Allouche, M. Oberkofler, M. Reinelt, and Ch. Linsmeier, "Quantum modeling of hydrogen retention in beryllium bulk and vacancies", *J. Phys. Chem. C* **114**, 3588 (2010).

19. Pople, J. A.; Head-Gordon, M.; Raghavachari, K. *J. Chem. Phys.* **87**, 5968–5975 (1987).

20. Ruzsinszky, A.; Perdew, J. P.; Csonka, G. I. *J. Phys. Chem. A* **109**, 11015 (2005).

21. Perdew, J. P.; Burke, K.; Ernzerhof, M. *Phys. Rev. Lett.* **77**, 3865–3868 (1996).

22. Zhao, Y.; Truhlar, D. G. *J. Phys. Chem. A* **110**, 5121-5129 (2006).

23. Roeggen, I.; Veseth, L. *Int. J. Quantum Chem.* **101**, 201 (2005).

24. Schäfer, A.; Huber, C.; Ahlrichs, R. *J. Chem. Phys.* **100**, 5829–5836 (1994).

25. Zhao, Y.; Truhlar, D. G. *Theor Chem Account* **120**, 215–241 (2008).

26. T.H. Dunning; *J. Chem. Phys.* **90**, 1007 (1989).

27. Grimme, S. *J. Comp. Chem.* **27**, 1787–1799 (2006).

28. Becke, A. D. *J. Chem. Phys.* **98**, 5648–5652 (1993).

29. Lee, C.; Yang, W.; Parr, R. G. *Phys. Rev. B* **37**, 785–789 (1988).

30. Tao, J. M.; Perdew, J. P.; Staroverov, V. N.; Scuseria, G. E. *Phys. Rev. Lett.* **91**, 146401 (2003).

31. Staroverov, V.N., Scuseria, G.E, Tao, J., Perdew, J.P. *J. Chem. Phys.* **119**, 12129 (2003).

32. Zhao, Y.; Schultz, N. E.; Truhlar, D. G. *J. Chem. Phys.* **123**, 161103 (2005).

33. Gaussian 09, Revision C.01, M. J. Frisch, G. W. Trucks, H. B. Schlegel, G. E. Scuseria, M. A. Robb, J. R. Cheeseman, G. Scalmani, V. Barone, B. Mennucci, G. A. Petersson, H. Nakatsuji, M. Caricato, X. Li, H. P. Hratchian, A. F. Izmaylov, J. Bloino, G. Zheng, J. L. Sonnenberg, M. Hada, M. Ehara, K. Toyota, R. Fukuda, J. Hasegawa, M. Ishida, T. Nakajima, Y. Honda, O. Kitao, H. Nakai, T. Vreven, J. A. Montgomery, Jr., J. E. Peralta, F. Ogliaro, M. Bearpark, J. J. Heyd, E. Brothers, K. N. Kudin, V. N. Staroverov, R. Kobayashi, J. Normand, K. Raghavachari, A. Rendell, J. C. Burant, S. S. Iyengar, J. Tomasi, M. Cossi, N. Rega, J. M. Millam, M. Klene, J. E. Knox, J. B. Cross, V. Bakken, C. Adamo, J. Jaramillo, R. Gomperts, R. E. Stratmann, O. Yazyev, A. J. Austin, R. Cammi, C. Pomelli, J. W. Ochterski, R. L. Martin, K. Morokuma, V. G. Zakrzewski, G. A. Voth, P. Salvador, J. J. Dannenberg, S. Dapprich, A. D. Daniels, Ö. Farkas, J. B. Foresman, J. V. Ortiz, J. Cioslowski, and D. J. Fox, Gaussian, Inc., Wallingford CT, 2009.

34. M. Šulka, D. Labanc, M. Kováč, M. Pitoňák, I. Černušák and P. Neogrády, *J. Phys. B: At. Mol. Opt. Phys.* **45**, 085102 (2012).

35. K. Eichkorn, O. Treutler, H. Öhm, M. Häser, and R. Ahlrichs, *Chem. Phys. Lett.* **240**, 283 (1995).

36. S. Nosé, *J. Chem. Phys.* **81**, 511 (1984); W. G. Hoover, *Phys. Rev. A* **31**, 1695 (1985).

37. TURBOMOLE Version 5.6, Universitat Karlsruhe, 2000.

38. G. J. Brendel, C. M. Marlett, and L. M. Niebylski "Crystalline Beryllium Hydride" , Inorganic Chemistry **17**, 3589 (1978)

39. T. J. Tague, Jr., and L. Andrews "Reactions of Beryllium Atoms with Hydrogen. Matrix Infrared spectra of Novel Product Molecules" , J. Am. Chem. Soc. **115**, 12111 (1993)